PROCEEDINGS OF SCIENCE

Standard-model prediction for direct CP violation in $K \to \pi\pi$ decays

C. Kelly*
RIKEN-BNL Research Center, Brookhaven National Laboratory, Upton, NY 11973, USA.
E-mail: ckelly@quark.phy.bnl.gov

We discuss our recent publication (Phys. Rev. Lett. 115 (2015) 21, 212001) of the first lattice QCD calculation of the complex kaon decay amplitude A_0 with physical kinematics, using a single $32^3 \times 64$ domain wall ensemble with G-parity spatial boundary conditions. We obtain approximate agreement with the experimental value for $\mathrm{Re}(A_0)$, which serves as a test of our method. Our prediction of $\mathrm{Im}(A_0)$ can be used to compute the direct CP violating ratio $\mathrm{Re}(\varepsilon'/\varepsilon)$, which we find to be $\sim 2\sigma$ lower than the experimental value. This result provides a new test of the Standard Model theory of CP violation, one which can be made more accurate with increasing computer capability.

The 33rd International Symposium on Lattice Field Theory
14 -18 July 2015
Kobe International Conference Center, Kobe, Japan

*Speaker.

PoS(LATTICE 2015)009

1. Introduction

Direct CP-violation was first observed in the late 1990s at CERN and FermiLab with the demonstration of a non-unit value for the ratio of decay amplitudes $|\eta_{00}/\eta_{\pm}|$, where $\eta_{ij} = A(K_L \to \pi_i\pi_j)/A(K_S \to \pi_i\pi_j)$. This is related to the measures of direct and indirect CP-violation, ε' and ε respectively, as follows:

$$\mathrm{Re}(\varepsilon'/\varepsilon) \approx \frac{1}{6}\left(1 - \left|\frac{\eta_{00}}{\eta_{\pm}}\right|^2\right) = 16.6(2.3) \times 10^{-4},$$

where the number is the experimental value. The small size of ε' ($\mathcal{O}(10^{-6})$) makes it highly sensitive to new, beyond the Standard Model sources of CP violation that may explain the origin of the matter-antimatter asymmetry in the Universe.

In terms of isospin the $K \to \pi\pi$ decays proceed via two allowed decay channels: a $\Delta I = 3/2$ decay to an $I = 2$ final state, and a $\Delta I = 1/2$ decay to an $I = 0$ state, the amplitudes of which are denoted A_2 and A_0 respectively. ε' is related to a difference in their complex phases:

$$\varepsilon' = \frac{i\omega e^{i(\delta_2 - \delta_0)}}{\sqrt{2}}\left(\frac{\mathrm{Im}(A_2)}{\mathrm{Re}(A_2)} - \frac{\mathrm{Im}(A_0)}{\mathrm{Re}(A_0)}\right). \tag{1.1}$$

While the underlying physics are high-energy $\Delta S = 1$ weak interactions at the $\sim$80 GeV scale, these decays receive substantial corrections from low-energy QCD interactions at the GeV scale and below. For example, a long-standing puzzle was the origin of the so-called $\Delta I = 1/2$ rule: the observation that neutral kaons are $\sim$450 times more likely to decay in the $\Delta I = 1/2$ channel than the $\Delta I = 3/2$. This corresponds to $\mathrm{Re}(A_0)/\mathrm{Re}(A_2) \simeq 22.5$. While a factor of $\sim$2 can be explained by the perturbative running from the weak to the hadronic scales, the origin of the remaining factor of $\sim$10 remained a mystery for several decades. In recent years the RBC and UKQCD collaborations have demonstrated that it likely arises due to a strong cancellation between the two dominant non-perturbative hadronic contributions to the $\Delta I = 3/2$ decay amplitude [1].

It is therefore vital to correctly describe the low-energy dynamics of these decays. Phenomenological calculations suffer from difficulties in assessing *a priori* the size of their systematic errors. On the other hand, lattice QCD provides an *ab initio*, systematically improvable technique for studying these non-perturbative effects.

These proceedings detail the RBC & UKQCD collaboration's recent lattice determination of ε' [2]. We begin by discussing the computational strategy, then discuss the ensemble used for the calculation. This is followed by an in-depth discussion of the fits to the matrix elements and $\pi\pi$ two-point functions. We conclude with a discussion of the systematic errors.

2. Summary of lattice approach

At the weak scale there are three classes of diagram that contribute to the $K \to \pi\pi$ decays: the current-current (Fig. 1a), QCD penguin (Fig. 1b) and the electroweak penguin (Fig. 1c) diagrams. At low-energy these are described very precisely by the following effective Hamiltonian:

$$H_W = \frac{G_F}{\sqrt{2}} V_{ud}^* V_{us} \sum_{j=1}^{10} [z_j(\mu) + \tau y_j(\mu)] Q_j(\mu).$$

Here z_j and y_j are perturbatively-computed Wilson coefficients encapsulating the high energy behavior. $\tau = -\frac{V_{ts}^* V_{td}}{V_{us}^* V_{ud}} = 0.0014606 + 0.00060408i$ is the only term with an imaginary part and is responsible for the CP violation. Q_j are 10 local effective four-quark operators: Q_1 and Q_2 correspond to the current-current diagrams, $Q_3 - Q_6$ the QCD penguin diagrams and $Q_7 - Q_{10}$ the electroweak penguin diagrams. The current-current operators Q_1 and Q_2 give the dominant contributions to the real parts of both A_0 and A_2; the QCD penguins Q_4 and Q_6 dominate $\mathrm{Im}(A_0)$;

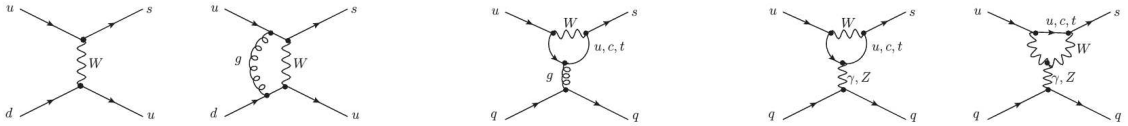

(a) Current-current (b) QCD penguin (c) Electroweak penguin

Figure 1: Weak-scale diagrams contributing to $K \to \pi\pi$ decays.

and the electroweak penguin operator Q_8 dominates $\mathrm{Im}(A_2)$. Note that only 7 of the 10 operators are linearly independent, hence it is sometimes convenient during the calculation to work in the 7-operator 'chiral basis' defined in Ref. [3].

On the lattice we compute the non-perturbative matrix elements of the four-quark operators between kaon and $\pi\pi$ states: $M_i^{I,\mathrm{lat}} = \langle (\pi\pi)_I | Q_i | K \rangle$ where $I = 0, 2$ is the isospin quantum number of the $\pi\pi$ final state. These are determined via the following three-point functions:

$$\langle J_{\pi\pi}(t_{\pi\pi}) Q_i(t_Q) J_K(t_K) \rangle = e^{-E_{\pi\pi}(t_{\pi\pi}-t_Q)} e^{-m_K(t_Q-t_K)} \langle 0|J_{\pi\pi}(0)|\pi\pi\rangle \langle \pi\pi|Q_i|K\rangle \langle K|J_K(0)|0\rangle + \dots , \tag{2.1}$$

after dividing out the source normalization computed from the corresponding two-point function:

$$\langle 0|J_X^\dagger(t_a) J_X(t_b)|0\rangle = e^{-E_X(t_a-t_b)} \, |\langle 0|J_X(0)|X\rangle|^2 + \dots , \tag{2.2}$$

where $X = \pi\pi$ or K. In the above J_X are appropriately chosen operators that overlap with the states of interest, and the ellipses indicate the presence of excited state contributions and, for Green's function containing the $I = 0$ $\pi\pi$ state, the contribution of the vacuum intermediate state.

The operator matrix elements must be renormalized in the same scheme as used to compute the Wilson coefficients; typically this is the $\overline{\mathrm{MS}}$ scheme, which involves dimensional regularization and is therefore not appropriate for a lattice calculation. Instead we utilize variants of the Rome-Southampton regularization-invariant momentum schemes [4] with non-exceptional kinematics [5] (RI/SMOM) as an intermediate scheme, with coefficients computed at an energy scale low enough to avoid discretization effects but sufficiently high to allow a subsequent perturbative matching to the $\overline{\mathrm{MS}}$ scheme [3]. In this calculation the one-loop truncation of the perturbative series used to compute these matching factors is one of the dominant sources of systematic error.

The amplitudes are obtained by combining the renormalization factors (which form a matrix due to operator mixing) with the lattice matrix elements and Wilson coefficients as follows:

$$A_I = F \frac{G_F}{\sqrt{2}} V_{ud}^* V_{us} \sum_{i,j=1}^{10} \left(z_i(\mu) + \tau y_i(\mu) \right) Z_{ij}^{\mathrm{lat}\to\overline{\mathrm{MS}}}(\mu) M_j^{I,\mathrm{lat}} . \tag{2.3}$$

Here the only new ingredient is the Lellouch-Lüscher factor F [6] that relates finite-volume matrix elements to infinite-volume amplitudes:

$$F^2 = 8\pi q \left(\frac{\partial \phi}{\partial q} + \frac{\partial \delta}{\partial q} \right) \frac{m_K E_{\pi\pi}^2}{p^3} \tag{2.4}$$

where $p = \sqrt{E_{\pi\pi}^2 - m_\pi^2}$ and $q = pL/2\pi$ where L is the lattice size. ϕ is a known analytic function and δ is the $\pi\pi$ scattering phase shift, the derivative of which must be determined either on the lattice or via phenomenology. For A_2 the derivative of ϕ dominates and we need only estimate the phase-shift derivative; however for A_0 the terms are comparable in size and the procedure by which the derivative is determined becomes a significant source of systematic error.

In order to determine physically-relevant quantities it is vital to simulate with physical kinematics, i.e. the energy of the two-pion state must match that of the kaon. For physical particles, the kaon mass $m_K \simeq 500$ MeV is considerably larger than the lightest two-pion state of energy $2 \times m_\pi \sim 270$ MeV (ignoring finite-volume interactions). A physical decay can therefore only be

achieved via an excited two-pion state in which the pions are non-stationary in the kaon rest frame. On the lattice these contributions are highly subdominant and in a conventional setup can only be extracted with multi-exponential fits to the time dependence, likely coupled with a careful choice of $\pi\pi$ operators. This strategy is made much more difficult for A_0 by the presence of disconnected diagrams in which the two pions annihilate into the vacuum and re-appear at a later time. These diagrams are highly susceptible to gauge-field noise and ultimately dominate the statistical error. An alternative approach is to take advantage of the freedom to choose the quark spatial boundary conditions (BCs) by choosing those that eliminate the stationary pion state; it is this approach that we adopt for our calculations.

3. Summary of A_2 determination

We begin by summarizing the most recent determination of A_2. This amplitude can be determined directly from the decay of charged kaons via

$$\langle (\pi^+\pi^0)_{I=2} | H_W | K^+ \rangle = \sqrt{2} A_2 e^{i\delta_2} .$$

Due to the absence of disconnected diagrams we can compute this quantity with high precision using standard lattice methods. The principle challenge is obtaining physical kinematics, which we achieve by imposing antiperiodic BCs on the down-quark propagators. Combined with up-quarks that satisfy standard periodic BCs, this results in charged pion states that are antiperiodic in space and therefore have allowed momenta that are odd-integer multiples of π/L. This eliminates the stationary ground-state but at the cost of explicitly breaking isospin (by applying different BCs to the up and down quarks). It also only applies to the charged pions, whereas the desired final state also contains a neutral pion. Both of these issues can be circumvented by applying the Wigner-Eckart relation to relate the above to the unphysical decay,

$$\langle (\pi^+\pi^0)_{I=2} | Q^{\Delta I_z = 1/2} | K^+ \rangle = \frac{\sqrt{3}}{2} \langle (\pi^+\pi^+)_{I=2} | Q^{\Delta I_z = 3/2} | K^+ \rangle ,$$

where the final state contains only charged pions and is protected from mixing with other isospin states by virtue of being the only charge-2 state with these quantum numbers.

Our first determination of A_2 [7, 8] was performed with physical masses and energy-conserving kinematics on a $32^3 \times 64 \times 32$ Shamir domain wall ensemble with the Iwasaki+DSDR gauge action [9] and a single, coarse lattice spacing of $a^{-1} = 1.378(7)$ GeV ($\beta = 1.75$) [10]. Here the dislocation-suppressing determinant ratio (DSDR) reduces the chiral symmetry breaking induced by 'dislocations' (tears) in the gauge field, which appear more frequently at strong coupling. An almost identical ensemble is used for our calculation of A_0 (this work).

Recently a significantly more precise determination [11] has been performed on our $48^3 \times 96 \times 24$ and $64^3 \times 128 \times 12$ Möbius domain wall ensembles with the Iwasaki gauge action and lattice spacings of $a^{-1} = 1.730(4)$ ($\beta = 2.13$) and $a^{-1} = 2.359(7)$ GeV ($\beta = 2.25$), respectively. Here we were able to take the continuum limit, eliminating the associated $\mathcal{O}(15\%)$ systematic error on the original measurement. In addition, using the all-mode averaging technique coupled with EigCG to generate the eigenvectors, we were able to compute the amplitude on these ensembles with a statistical precision of only $\sim 3\%$. The results are

$$\begin{aligned} \mathrm{Re}(A_2) &= 1.50(4)_{\mathrm{stat}}(14)_{\mathrm{sys}} \times 10^{-8} \\ \mathrm{Im}(A_2) &= -6.99(20)_{\mathrm{stat}}(84)_{\mathrm{sys}} \times 10^{-13} \end{aligned} \tag{3.1}$$

where the errors are statistical and systematic, respectively. We find excellent agreement with the experimental value for the real part, $\mathrm{Re}(A_2)_{\mathrm{expt}} = 1.4787(31) \times 10^{-8}$. The imaginary part is known only from these calculations.

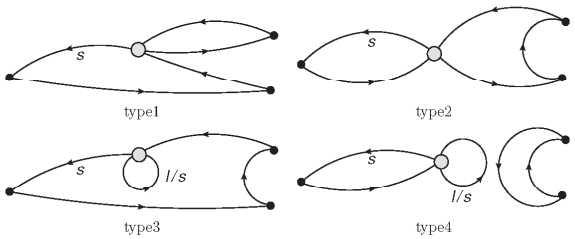

Figure 2: Examples of the four types of diagram contributing to the $\Delta I = 1/2$, $K \to \pi\pi$ decay. Lines labeled ℓ or s represent light or strange quarks. Unlabeled lines are light quarks.

The systematic errors are dominated by perturbative truncation errors in the computation of the Wilson coefficients and the matching from the non-perturbative RI/SMOM renormalization schemes to $\overline{\text{MS}}$. These errors can be reduced in the future either by computing higher-order perturbative contributions to these quantities or by step-scaling the RI/SMOM renormalization factors to a higher energy scale than the present $\mu = 3$ GeV.

4. Techniques for the determination of A_0

In order to obtain A_0 we must measure the decays of a neutral kaon into two-pion states comprising both charged ($\pi^+\pi^-$) and neutral ($\pi^0\pi^0$) pions. These give rise to roughly 50 distinct contraction topologies that are divided into the four-classes shown in Figure 2. Here the type-4 diagrams are the disconnected contributions that dominate the statistical error.

Aside from the large number of contractions, this calculation is significantly more challenging than that of A_2 for two further reasons: the presence of disconnected diagrams makes it necessary to employ advanced error-reduction techniques to manage the statistical error; and the simple approach to obtaining physical kinematics used for the A_2 calculation is not applicable to A_0 and a more sophisticated technique is required. Below we describe how these two issues are addressed.

4.1 Disconnected diagrams

A significant amount of the $\pi\pi$ vacuum coupling can be eliminated by separating the pion sources in Euclidean time, a refinement first introduced in Ref. [12]. Further suppression can be achieved by combining the quark and anti-quark fields into "meson wavefunctions" constructed in our case from hydrogen atom wavefunctions. The remaining statistical error can be reduced by averaging over all spatial locations of the two-pion wavefunctions. These two steps are made possible by employing the all-to-all propagator technique of Ref. [13] whereby an approximation to the propagator from any site to any other is obtained by first computing a subset of exact eigenmodes of the Dirac matrix using, for example, the Lanczos algorithm, and 'patching up' the remaining, typically less important, high-mode contributions using a stochastic technique. In this approach one can optionally 'dilute' the stochastic sources in the spin, color, and in our case flavor indices, in order to reduce the reliance on stochastic cancellation to correctly describe the index structure of the propagator on a given site, at the cost of increasing the number of inversions and the memory footprint. In practice we dilute in all three of these indices, and additionally dilute in the source time coordinate to improve the temporal resolution.

4.2 Physical kinematics

For A_0 we must compute both $K^0 \to \pi^+\pi^-$ and $K^0 \to \pi^0\pi^0$ decays. As in the A_2 calculation, some of the final states contain neutral pions that remain stationary when we impose antiperiodic BCs on the down quark. Unfortunately, in the $I = 0$ case there is no Wigner-Eckart relation that can be used to work around this issue as well as to protect us from isospin breaking. Following Ref. [14] we instead apply G-parity spatial boundary conditions (GPBC) [15, 14, 16] to achieve the

desired effect. G-parity is the combined action of charge conjugation and an 180-degree isospin rotation about the y-axis: $\hat{G} = \hat{C}e^{i\pi\hat{I}_y}$, where the hat-symbol is used to denote operators. The charged and neutral pions are G-parity odd, thus applying the operation at a spatial boundary is equivalent to imposing antiperiodic boundary conditions on the pions, again resulting in momenta that are odd-integer multiples of π/L.

At the quark level,

$$\hat{G}\begin{pmatrix} u \\ d \end{pmatrix}\hat{G}^{-1} = \begin{pmatrix} -C\bar{d}^T \\ C\bar{u}^T \end{pmatrix}, \tag{4.1}$$

where $C = \gamma^2\gamma^4$ in our conventions. This flavor mixing at the boundary introduces a number of difficulties that we had to overcome [17, 18, 19, 20]. In summary,

- Consistency across the boundary between the u and d quarks, which couple to the standard gauge links U, and their G-parity partners $\bar{d}^T$ and $\bar{u}^T$ which couple to the complex-conjugate links U^*, requires the gauge field to obey complex conjugate (charge conjugation) BCs. This requires the generation of custom ensembles.

- Quark propagators spanning the boundary introduce unusual Wick contractions between oppositely-flavored spinor fields $\overbrace{du}^T$ and conjugate spinors $\overbrace{\bar{u}^T\bar{d}}$. This results in a number of additional diagrams that must be evaluated for a given Green's function.

- For GPBC in two or more directions the hypercubic rotational symmetry is broken at the quark level, manifesting as restrictions on the allowed values of discretized quark momenta. Although this symmetry is respected at the pion level (these just obey antiperiodic BCs), the restrictions on the quark momenta prevent us from forming $\pi\pi$ operators for pions moving along orthogonal axes that are related by rotations. As the Lüscher formalism requires that the $\pi\pi$ states reside in the A_1 representation of the hypercubic group we must treat this issue with care. In practise we found [19, 20] that a careful choice of pion operator heavily suppresses the breaking to below the level of statistical resolution.

- The neutral kaon states, $K^0 = d\bar{s}$ and $\bar{K}^0 = s\bar{d}$, are not eigenstates of the system as GPBC transforms the down quark but not the strange. In addition, modifications to the strange-quark Lagrangian are required for consistency with the charge-conjugation BCs on the gauge fields. The solution is to impose GPBC on an isospin doublet comprising the s-quark and a fictional, degenerate quark field s'. The operator, $\tilde{K}^0 = \frac{1}{\sqrt{2}}(d\bar{s} + \bar{u}s')$ is then G-parity even and hence projects only onto states with zero momentum.

  For the $K \to \pi\pi$ interaction we use the physical four-quark operators, which act solely on the $d\bar{s}$ component and hence couple only to the $\bar{u}s'$ through terms that are exponentially suppressed in the kaon mass and lattice size.

  In order to revert to a three flavor simulation we must take the square-root of the s/s' determinant that represents the fermionic contribution to the path integral. Due to the coupling between the fields at the boundary, this results in a non-local determinant that potentially introduces universality violations; however, it can be shown that such effects are exponentially suppressed in the lattice size.

5. Ensemble details and basic measurements

We perform this first determination of A_0 using a single $32^3 \times 64$ domain wall ensemble with the Iwasaki+DSDR gauge action at $\beta = 1.75$. This is essentially identical to the ensemble used for

the original A_2 determination and described above, apart from in the following regards: Firstly we reduced the input quark mass from 1×10^{-3} to 1×10^{-4} in order to obtain physical pion masses; secondly we switched from Shamir DWF with $L_s = 32$ to Möbius DWF with $L_s = 12$ and $b + c = 32/12$, the latter of which has the same degree of chiral symmetry breaking as the former but costs substantially less to generate; and finally we use GPBC for the sea quarks. One benefit of choosing the same parameters as an existing ensemble is that we can use that ensemble to obtain the renormalization factors for the $K \to \pi\pi$ matrix elements free from the difficulties of GPBC, which, like all boundary conditions, have no impact on high-energy observables and would serve only to further complicate the calculation.

Although the lattice spacing of this ensemble is coarse, with $a^{-1} = 1.378(7)$ GeV, we attain a large physical box size of $(4.6 \text{ fm})^3$ without having to simulate with a large number of lattice sites (for example the $64^3 \times 128$ lattice size used in our recent A_2 calculation). This is particularly important here because GPBC introduce a naïve factor of two increase in the cost of inversions due to the double-sized (two-flavor) Dirac matrix. Additional overheads arise because the square of this operator, which is used as the kernel of the CG inversion in order to guarantee hermiticity and positive-definiteness, represents four flavors of quarks; we must therefore take the square-root of the light-quark determinant in order to simulate with two light flavors. This requires the use of the RHMC algorithm, for which the underlying multi-shift CG has a substantial linear algebra overhead over traditional CG which results in a significant reduction in performance on the IBM Blue Gene/Q machines used for this calculation.

For this calculation we make use of 216 configurations separated by 4 MD time units. The ensemble generation and subsequent measurements were performed using the following IBM Blue Gene/Q installations: the 512-node USQCD machine at BNL, the US DOE "Mira" machine at ANL and the STFC "DiRAC" machine at Edinburgh, UK. The computational cost of each measurement (4 configurations plus 1 measurement) is approximately 1 BG/Q rack-day, and the calculation required roughly 200M BG/Q core-hours in total.

All measurements were performed using the all-to-all propagators. As mentioned above we dilute in all indices (spin, color, flavor and time), and we use one stochastic hit per configuration.

In order to examine the effects of autocorrelations between configurations we performed a binning analysis using several quantities, from which we observed no bin size dependence. This is not unreasonable given that it is such a coarse lattice. As a result all of our measurements are performed without binning the data.

We fit both the pion and kaon two-point functions using uncorrelated fits. The data were folded (averaged) about $t = 32$ and fit to $6 \leq t \leq 32$. The fits to the $\pi\pi$ two-point function were more challenging, and will be discussed in more detail below. The measured masses and energies are given in Table 1. We obtain a pion ground-state energy consistent with the physical pion mass as desired, and we observe excellent agreement between the measured $I = 0$ $\pi\pi$ energy and the kaon mass, thereby achieving our goal of energy conserving kinematics in the $K \to \pi\pi$ decay.

6. Determination of the $I = 0$ $\pi\pi$ energy

The Wick contractions for the $I = 0$ $\pi\pi$ two-point function

$$C(t) = \langle 0 | J^{\dagger}_{\pi\pi}(t) J_{\pi\pi}(0) | 0 \rangle$$

are given in Fig. 3. Here the 'V'-diagrams are disconnected and dominate the noise.

Here and for the $K \to \pi\pi$ matrix elements below we use ground-state hydrogen atom wave-function sources for the pions with a radius of 2 in lattice units, and we separate the sources by 4 timeslices in order to reduce the coupling to the vacuum. Despite these efforts, the dominant

Quantity	Value
m_K	490.6(2.4) MeV
$E_{\pi\pi}(I=0)$	498(11) MeV
E_π	274.6(1.4) MeV
(m_π	143.1(2.0) MeV)

Table 1: Measured energies of the kaon, pion and $\pi\pi$ states. The value of m_π on the final line was obtained by applying the continuum dispersion relation $m_\pi^2 = E_\pi^2 - 3\frac{\pi^2}{L^2}$ to the measured moving-pion energy.

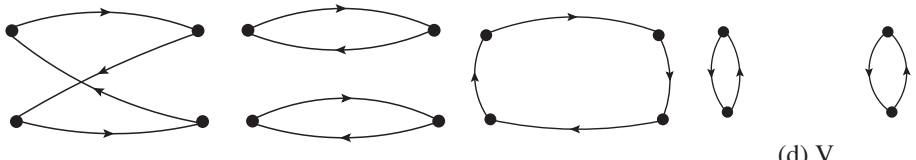

(a) C (b) D (c) R (d) V

Figure 3: The four Wick contractions for the $I=0$ $\pi\pi$ two-point function. The subcaption indicates the label we assign to each diagram. The black circles on the left and right of each diagram are the pion destruction and creation operators respectively, which are separated in time along the x-axis and in space along the y-axis. In practise we separate the two source (and sink) operators in time to reduce the vacuum coupling, although this is not shown in this figure.

contribution to the amplitude remains the vacuum intermediate state (by roughly a factor of 10), and therefore a subtraction is required. For these two-point functions this can be achieved either by direct subtraction,

$$C_{\text{sub}}(t) = \langle 0|J^\dagger_{\pi\pi}(t)J_{\pi\pi}(0)|0\rangle - \langle 0|J^\dagger_{\pi\pi}(t)|0\rangle\langle 0|J_{\pi\pi}(0)|0\rangle\,,$$

or by appending an additional constant term to the fit function Eq. 2.2 and allowing the fit to determine the vacuum contribution; both approaches give consistent results. Such a constant term also arises due to round-the-world effects in which one pion propagates backwards through the boundary while the other propagates in the forwards direction, although in practise we found this contribution to be statistically consistent with zero after the vacuum subtraction was performed.

We observed strong correlations between values of the two-point function at different times, necessitating the use of correlated fits – fortunately the condition number was small enough, $\mathcal{O}(1\times 10^4)$, that the correlation matrix could be reliably inverted. In order to properly take into account the fluctuations in the correlation matrix between jackknife samples we compute separate matrices for each sample using the double-jackknife technique.

In Fig. 4 we plot the effective energy of the $\pi\pi$ state. We observe a rapid deterioration of the signal-to-noise ratio, which implies that any single-exponential fit will be dominated by the lowest one or two points in the fit window. This makes it very difficult to separate the effects of statistical fluctuations in the data from any actual underlying time dependence arising from excited state contamination. Indeed when we perform single-exponential fits, varying the lower bound above the apparent onset of the plateau region at $t=4$, we observe fluctuations in the fitted energies (Table 2) that closely mirror the temporal fluctuations in the two-point effective energy seen in the figure. To clarify the situation we also performed double-exponential fits with several different t_{min}, the results of which are also given in the table. While this approach gives larger errors, the measured ground-state energies agree well and are all somewhat lower than the values obtained

$t_{\min}$	$E_{\pi\pi}$	χ^2/dof
4	0.377(4)	2.1(8)
5	0.376(6)	2.2(8)
6	0.361(7)	1.6(7)
7	0.379(11)	1.3(6)

$t_{\min}$	$E_{\pi\pi}$	E_{exc}	χ^2/dof
2	0.363(9)	1.04(17)	1.7(7)
3	0.367(11)	1.27(73)	1.8(8)
4	0.364(12)	0.86(39)	1.9(8)

Table 2: Results of single-exponential (left) and double-exponential (right) to the $I = 0$ $\pi\pi$ two-point function, varying the lower bound of the fit, $t_{\min}$.

from the single-exponential fits with $t_{\min} \leq 5$ (this is also the case for $t_{\min} = 7$ but we judge this to be a statistical fluctuation based on Fig. 4). Given that the fitted excited-state energies are all in good agreement, we take these lower ground-state energies as evidence of a small underlying excited-state contamination in the region $t \leq 5$. We therefore choose the single-exponential fit with $t_{\min} = 6$ as our final value, for which $E_{\pi\pi} = 0.361(7)$ in lattice units or 498(11) MeV in physical units.

As discussed in Ref. [21], the expected finite-volume $\pi\pi$ energy for a lattice with our size and BCs can be estimated by matching the Lüscher formula [22] (appropriately modified for antiperiodic spatial boundary conditions on the pion [23, 11]) with phenomenological curves [24, 25] of the energy dependence of the phase shift based on the Roy equations and experimental measurements of the scattering lengths and the phase shift at high energies. This gives a value of $E_{\pi\pi} \approx 470$ MeV, $\sim 3\sigma$ smaller than our result. Correspondingly, our phase shift, $\delta_0 = 23.8(4.9)(1.2)^\circ$, is smaller than the $38.0(1.3)^\circ$ obtained for our pion mass from phenomenology [26, 25]. The origin of this discrepancy requires further investigation.

If the lattice calculation presented here is the source of this discrepancy, it would likely arise from the two dominant systematic effects: the lattice discretization and possibly further excited state contamination hidden by the rapidly decreasing signal-to-noise ratio.

One source of discretization error is associated with the use of the continuum dispersion relation ($E^2 = \vec{p}^2 + m^2$) rather than the lattice relation to determine am_π and the Lüscher momentum q that parameterizes the interaction energy. Ref. [27] provides a modified form appropriate for Gaussian fields on the lattice:

$$\cosh(E) = 2\textstyle\sum_i \sin^2(p_i/2) + \cosh m\,.$$

With this relation we find $\delta_0 = 23.9^\circ$, only 0.1° larger than our previous quoted value. This change is small compared to the statistical error and can therefore be neglected. An additional source of error arises due to discretization corrections to the Lüscher zeta function. Such effects are known to be exponentially suppressed in the lattice size and pion mass (cf. e.g. [28]). In our case the GPBC causes the pion mass to be replaced by the ground-state energy, for which $E_\pi L = 6.38$, and therefore we might expect corrections $\mathcal{O}(0.2\%)$. Of course the coefficient of such terms is unknown, therefore we choose a more conservative estimate whereby the phase shift is assigned a $\mathcal{O}(5\%)$ discretization error based on that measured for a number of other physical observables on this coarse lattice [9]. This is the origin of the 1.2° systematic in the value quoted above.

As previously stated our two-state fits showed excellent consistency in their determination of the ground-state energy and therefore we have no evidence of further excited state contamination. While we cannot yet rule out such a nearby excited state, such a state is not predicted by the conventional phenomenological analysis and its presence would represent an equally serious failure of current phenomenological expectations. At present we do not assign a systematic error to this possibility, but we expect that the situation will be clarified with more statistics.

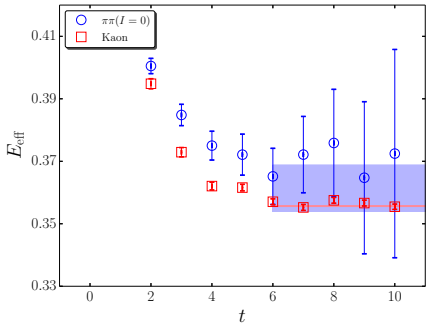

Figure 4: Effective energies of the kaon (squares) and two-pion (circles) states deduced from the corresponding two-point functions by equating the results from two time separations to the function $A\cosh E_{\rm eff}(T/2-t)$ where $T=64$ is the temporal lattice size, plotted as a function of the smallest of those two separations. (We replace T by $T-8$ for the $\pi\pi$ case.) These are overlaid by the errorbands corresponding to the fitted values of $E_{\pi\pi}$ (light blue) and m_K (pink).

7. Lellouch-Lüscher factor

The phase shift enters the determination of the $K \to \pi\pi$ amplitudes via the Lellouch-Lüscher (LL) formula Eq. 2.4 as a derivative with respect to the binding energy. We observe that changing the phase between the lattice and phenomenological value results only in a 4% change in the amplitude; much smaller than the other systematic errors in the problem (including the determination of the derivative itself - cf. below). We therefore proceed using the lattice value.

In Ref. [5] it was recognized that the derivative of the zeta-function ϕ dominates the LL factor for the $\Delta I = 3/2$ decays, therefore it was sufficient to make use of the scattering length approximation, which states that the phase shift depends linearly on q at low energies, i.e. $\frac{\partial\delta}{\partial q} = \frac{\delta}{q}$. From the phenomenological curves [24, 25] it is clear that the derivative of δ_0 is much larger than δ_2. We must therefore treat the determination of the phase-shift derivative with more care. In absence of a second lattice momentum we cannot compute this directly and instead consider three choices:

1. Using the scattering length approximation: $\frac{\partial\delta}{\partial q} = 0.55(13)$ (with the numerator in radians).
2. Taking the derivative of the phenomenological fit in Refs. [24]: $\frac{\partial\delta}{\partial q} = 1.54(3)$.
3. Using a linear approximation in $E_{\pi\pi} - 2m_\pi$ inspired by the strong linearity of the phase shifts in the above phenomenological curves: $\frac{\partial\delta}{\partial q} = 0.87(21)$.

We prefer to base our final value on pure-lattice numbers and therefore take the scattering-length approximation for our central value, giving $F = 23.96(61)$. The full 11% spread in F is included as a systematic error.

8. $K \to \pi\pi$ matrix element fits

We generated the three-point functions with five different $t_{\pi\pi} - t_K$ separations: 10, 12, 14, 16, 18. In Figure 5 we show the effective lattice amplitudes for Q_2 and Q_6, which are the dominant contributions to the real and imaginary parts of A_0, respectively. These figures were obtained by performing the error-weighted average over the five time separations. For the fits themselves we fit all five time separations simultaneously with a common matrix element amplitude.

Prior to fitting we must account for an unphysical, quadratically-divergent contribution that arises because the type-3 and type-4 diagrams of Figure 2 mix with the dimension-3 operator $\bar{s}\gamma^5 d$. This operator is the divergence of an axial current hence its matrix elements vanish when the

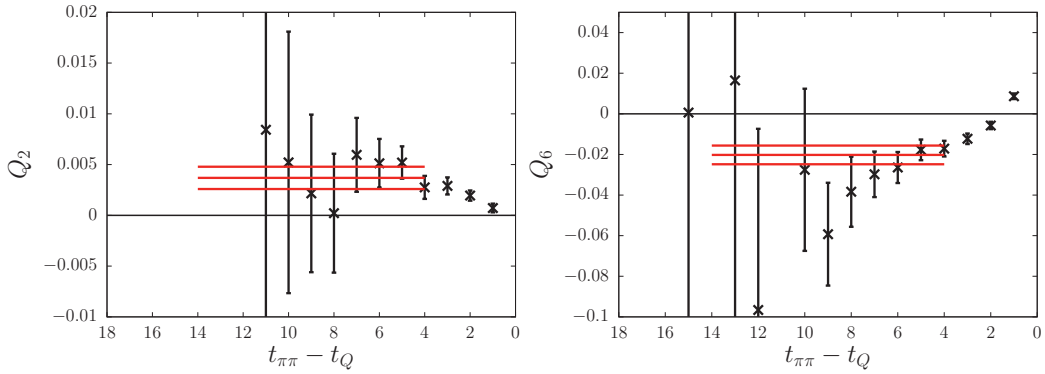

Figure 5: The Q_2 and Q_6 three-point functions, plotted in lattice units as functions of $t_{\pi\pi} - t_Q$, with the time dependence in Eq. 2.1 removed. The horizontal lines show the central value and errors from the fit described below.

four-momenta of the kaon and $\pi\pi$ are equal; it will therefore not contribute to a physical process. However, for matrix elements with unphysical kinematics this term may be $20\times$ larger than the other, physical terms. Even with physical kinematics it will introduce both noise and increased systematic error due to contamination from excited states with energies larger than the kaon mass. We remove this contribution by computing the amplitudes with subtracted operators [29, 5], $Q_i^{\text{sub}} = Q_i - \alpha_i \bar{s}\gamma^5 d$, where the coefficients α_i are chosen such that the following expression is satisfied:

$$\langle 0|Q_i - \alpha_i \bar{s}\gamma^5 d|K\rangle = 0\,.$$

These coefficients are time independent, but in practise we obtained smaller statistical errors on the subtracted matrix elements by performing the subtraction timeslice-by-timeslice, i.e. by computing α_i separately for each timeslice t and using those coefficients in the subtraction for $Q_i(t)$. The subtraction leaves behind an unphysical, regulator dependent $\bar{s}\gamma^5 d$ piece, but one that is no longer $1/a^2$ enhanced and is therefore small providing we tune the kaon and $\pi\pi$ energies sufficiently well. We include this potential effect as an 'unphysical kinematics' systematic error below.

Note that both the type-4 diagrams, and the corresponding diagrams in which Q_i is substituted for $\bar{s}\gamma^5 d$, require a vacuum subtraction which here must be computed directly.

In order to isolate the ground-state contribution we must impose a lower bound on the separation between the four-quark operator and the $\pi\pi$ sink ($t_{\pi\pi} - t_Q$). We found that bounds of $3, 4, 5$ and 6 all gave results consistent within statistics. Given how rapidly the signal degenerates we chose a lower bound of $t_{\pi\pi} - t_Q = 4$, smaller than the $\pi - \pi$ separation of 6 used for the two-point function. We include the possibility of any remaining excited state contamination in our systematic error budget, below. We also use a minimum $t_Q - t_K = 6$, consistent with that used for the kaon two-point function. The total number of data points included in the fit is 25. We performed uncorrelated fits but experiments with correlated fits gave consistent results.

Table 3 shows the unrenormalized matrix elements written in the traditional, physical basis and in the chiral basis. For convenience we have converted the values into physical units and have applied the Lellouch-Lüscher finite-volume correction of $F = 23.96(61)$ to obtain infinite-volume matrix elements with the operator conventions specified in Ref. [8].

9. Renormalization factors and Wilson coefficients

The $\overline{\text{MS}}$-renormalized operators are computed by first converting to the RI/SMOM$(\not{q}, \not{q})$

i	$\mathscr{M}^{(i)}_{\rm lat}$ (GeV)^3	$\mathscr{M}'^{(i)}_{\rm lat}$ (GeV)^3
1	-0.247(62)	-0.147(242)
2	0.266(72)	-0.218(54)
3	-0.064(183)	0.295(59)
4	0.444(189)	—
5	-0.601(146)	-0.601(146)
6	-1.188(287)	-1.188(287)
7	1.33(8)	1.33(8)
8	4.65(14)	4.65(15)
9	-0.345(97)	—
10	0.176(100)	—

i	$\mathscr{M}'^{(i)}_{\rm SMOM}$ (GeV)^3	$\mathscr{M}^{(i)}_{\overline{\rm MS}}$ (GeV)^3
1	-0.0675(1109)(128)	-0.151(29)(36)
2	-0.156(27)(30)	0.169(42)(41)
3	0.212(52)(40)	-0.0492(652)(118)
4	—	0.271(93)(65)
5	-0.193(62)(37)	-0.191(48)(46)
6	-0.366(103)(70)	-0.379(97)(91)
7	0.225(37)(43)	0.219(37)(53)
8	1.65(5)(31)	1.72(6)(41)
9	—	-0.202(54)(49)
10	—	0.118(42)(28)

Table 3: Left: The unrenormalized matrix elements in the conventional ten-operator basis (second column) and the seven-operator chiral basis (third column). Only statistical errors are shown. Right: The renormalized matrix elements in the RI/SMOM$(\not{q},\not{q})$ scheme and chiral basis (second column) and resulting the $\overline{\rm MS}$ matrix elements in the traditional 10-operator basis. The left error shown is statistical and the right is systematic.

scheme [3] and then perturbatively matching to $\overline{\rm MS}$. The RI/SMOM schemes are defined in the 7-operator chiral basis, hence we must first perform a basis conversion (Table 3). These operators, Q'_j, are then renormalized to RI/SMOM operators, $Q^{\rm RI}_k$, by applying the 7×7 matrix with elements $Z^{\rm lat\to RI}_{jk}$. This matrix is computed by imposing the RI/SMOM$(\not{q},\not{q})$ renormalization conditions on amputated, Landau-gauge fixed Green's functions of Q'_j with off-shell, external momenta specified by the two momenta, p_1 and p_2. We use $p_1 = \frac{2\pi}{L}(0,4,4,0)$ and $p_2 = \frac{2\pi}{L}(4,4,0,0)$, which together satisfy the symmetric momentum condition $p_1^2 = p_2^2 = (p_1-p_2)^2 = (\mu)^2$, where $\mu = 1.531$ GeV is the renormalization scale. As previously mentioned, the renormalization factors are computed on our existing $32^3\times 64\times 32$ Shamir domain wall ensemble with the Iwasaki+DSDR gauge action. The choice of renormalization scale, $\mu = 1.531$ GeV, was dictated by the desire to avoid large discretization effects on this coarse lattice and is lower than the $\mathscr{O}(3$ GeV$)$ scale at which this procedure is typically applied, giving rise to a correspondingly larger systematic error.

The RI/SMOM$(\not{q},\not{q})$ NPR matrix and the one-loop perturbative matching matrix converting these to the $\overline{\rm MS}$ are given in Ref. [2] (Supplementary Material), and the renormalized operators in both schemes are given in Table 3.

The real and imaginary parts of A_0 are obtained by multiplying the $\overline{\rm MS}$-renormalized matrix elements by the appropriate Wilson coefficients and CKM matrix elements via Eq. 2.3. The Wilson coefficients were computed at the renormalization scale of $\mu = 1.531$ GeV from the equations given in Ref. [30]. We use the two-loop beta function to obtain the three-flavor value of $\alpha_S = 0.353388$ at $\mu = 1.531$ GeV. The values of the Wilson coefficients and the other phenomenological input entering their determination are given in Ref. [2] (Supplementary Material). The final contributions to ${\rm Re}(A_0)$ and ${\rm Im}(A_0)$ of each operator are given in Table 4, where the errors are statistical only.

10. Systematic errors

The systematic error budget for our calculation is given in Table 5. These errors are understood to apply separately and equally to each of the 10 operator contributions, and are treated as uncorrelated when the sum of the contributions is performed: The systematic error on the sum is taken as the largest of either the quadratic or linear combination of the individual error contributions.

Below we briefly describe how the systematic error estimates are determined, in order of descending importance:

i	Re(A_0)(GeV)	Im(A_0)(GeV)
1	$1.02(0.20)(0.07) \times 10^{-7}$	0
2	$3.63(0.91)(0.28) \times 10^{-7}$	0
3	$-1.19(1.58)(1.12) \times 10^{-10}$	$1.54(2.04)(1.45) \times 10^{-12}$
4	$-1.86(0.63)(0.33) \times 10^{-9}$	$1.82(0.62)(0.32) \times 10^{-11}$
5	$-8.72(2.17)(1.80) \times 10^{-10}$	$1.57(0.39)(0.32) \times 10^{-12}$
6	$3.33(0.85)(0.22) \times 10^{-9}$	$-3.57(0.91)(0.24) \times 10^{-11}$
7	$2.40(0.41)(0.00) \times 10^{-11}$	$8.55(1.45)(0.00) \times 10^{-14}$
8	$-1.33(0.04)(0.00) \times 10^{-10}$	$-1.71(0.05)(0.00) \times 10^{-12}$
9	$-7.12(1.90)(0.46) \times 10^{-12}$	$-2.43(0.65)(0.16) \times 10^{-12}$
10	$7.57(2.72)(0.71) \times 10^{-12}$	$-4.74(1.70)(0.44) \times 10^{-13}$
Tot	$4.66(0.96)(0.27) \times 10^{-7}$	$-1.90(1.19)(0.32) \times 10^{-11}$

Table 4: Contributions to A_0 from the ten continuum, $\overline{\text{MS}}$ operators $Q_i(\mu)$, for $\mu = 1.53$ GeV. Two statistical errors are shown: the first from the lattice matrix element and the second from the lattice to $\overline{\text{MS}}$ conversion.

Description	Error	Description	Error
Finite lattice spacing	12%	Finite volume	7%
Wilson coefficients	12%	Excited states	$\leq 5\%$
Parametric errors	5%	Operator renormalization	15%
Unphysical kinematics	$\leq 3\%$	Lellouch-Lüscher factor	11%
Total (added in quadrature)			27%

Table 5: Representative, fractional systematic errors for the individual operator contributions to Re(A_0) and Im(A_0).

Operator renormalization: Alongside the RI/SMOM($\not{q},\not{q}$) we also computed renormalization factors in the RI/SMOM(γ^μ,γ^μ) scheme. We examine the full difference of the result for each of the 10 operators and from these choose 15% as a representative number, which is large due to the relatively small renormalization scale of 1.531 GeV.

Wilson coefficients: For the same reason the error on the Wilson coefficients is also large. This is estimated conservatively by taking the full difference between the leading- and next-to-leading order values using the procedure described in Ref. [8].

Finite lattice spacing: We estimate this error by comparing the three individual contributions to A_2 between the original determination [7, 8] on a lattice nearly identical to that used in this work, and the continuum-limit contributions determined in Ref. [11]. The average of the fractional changes was used for our final error.

Lellouch-Lüscher factor: As discussed above we use the full spread in values of the phase-shift derivative to estimate this error.

Finite volume: We use the same estimate determined for A_2 in Ref. [8], which was estimated using SU(3) finite-volume chiral perturbation theory.

Parametric errors: These errors arise from the uncertainties on the inputs used in the determination of the amplitudes and is dominated by that of the ratio τ. We propagated the errors by hand to determine the final number.

Excited states: Using our two-state fits to the $\pi\pi$ two-point function we estimate the relative contribution of the excited-state to the amplitude at $t_{\pi\pi} - t_Q = 4$ (the lower bound on our three-point function fit); the same fractional error is assigned to the three-point function.

Unphysical kinematics: This error is associated with the slight mis-tuning between the kaon and $\pi\pi$ energies. To estimate it we repeated our measurement on a subset of configurations using a slightly larger strange quark mass. The fractional difference in central values between the best-resolved matrix element, that of Q_2, was scaled by the difference between our kaon and $\pi\pi$ energies to obtain the quoted figure.

We note that as the error on this calculation is dominated by the statistics, these systematic errors are not intended to be bounds but only reasonable estimates.

11. Results for A_0 and ε'

Adding the contributions to A_0 given in Table 4 and the systematic errors from the previous section, we find

$$\mathrm{Re}(A_0) = 4.66(1.00)(1.26) \times 10^{-7}\ \mathrm{GeV} \tag{11.1}$$

$$\mathrm{Im}(A_0) = -1.90(1.23)(1.08) \times 10^{-11}\ \mathrm{GeV} \tag{11.2}$$

where the errors are statistical and systematic, respectively. From these we obtain

$$\mathrm{Re}\left(\frac{\varepsilon'}{\varepsilon}\right) = \mathrm{Re}\left\{\frac{i\omega e^{i(\delta_2-\delta_0)}}{\sqrt{2}\varepsilon}\left[\frac{\mathrm{Im}A_2}{\mathrm{Re}A_2} - \frac{\mathrm{Im}A_0}{\mathrm{Re}A_0}\right]\right\} \tag{11.3}$$

$$= 1.38(5.15)(4.59) \times 10^{-4}, \tag{11.4}$$

where we have used $\mathrm{Im}(A_0)$ and δ_0 values given above and our earlier results for $\mathrm{Im}(A_2)$ and δ_2 [11]. We use the experimental values for $\mathrm{Re}(A_0)$, $\mathrm{Re}(A_2)$ and their ratio ω (since these are accurately determined from the measured $K \to \pi\pi$ decay rates) and the experimental value for ε.

12. Conclusions

In this document we have detailed the first determination of the direct CP violation parameter ε' with controlled errors. Our result for $\mathrm{Re}(\varepsilon'/\varepsilon)$ is broadly in agreement (2.1σ) with the experimental number but may, with continued effort, reveal a discrepancy indicating new physics. The focus of the present discussion is the calculation of A_0, for which we find the real part to be in good agreement with the experimental number (as expected), serving as a test of the method and demonstrating consistency with our earlier explanation of the $\Delta I = 1/2$ rule [1] in which the large ratio of $\mathrm{Re}(A_0)$/$\mathrm{Re}(A_2)$ resulted from a significant cancellation between the two dominant terms contributing to $\mathrm{Re}(A_2)$, a cancellation which does not occur for $\mathrm{Re}(A_0)$.

The errors are currently statistics-bound. This is particularly the case for $\mathrm{Im}(A_0)$ where we observe a strong cancellation between the contributions of the two dominant operators, Q_4 and Q_6, resulting in a 63% statistical error on their sum despite having only 34% and 24% relative errors on the two terms, respectively. More measurements are currently underway to reduce this error. Of the systematic errors the dominant contribution is due to the truncation of the perturbative series used to match the RI/SMOM renormalization scheme to $\overline{\mathrm{MS}}$, and also in the computation of the Wilson coefficients. These errors are exacerbated by the low, 1.531 GeV renormalization scale and we expect significant improvements through the use of step-scaling to a higher scale $\mathcal{O}(3\ \mathrm{GeV})$, a calculation which is also currently underway. Further study of the $\pi\pi$ phase shifts to determine the origin of the observed discrepancy between our result and phenomenology will be required in future, and also a study of the energy dependence of the phase shift to reduce the 11% error on the Lellouch-Lüscher factor. Additional lattice spacings will be required to reduce the discretization systematic. Ultimately we expect that within 5 years we will be able reduce the total relative error on $\mathrm{Re}(\varepsilon'/\varepsilon)$ to the level of 10%, and further refinemenrs will become possible with increased computer power and the inclusion of electromagnetism and isospin-breaking effects.

13. Acknowledgements

We would like to thank our RBC and UKQCD collaborators for helpful discussions and support. This calculation was carried out under the INCITE Program of the US DOE on the IBM Blue Gene/Q (BG/Q) Mira machine at the Argonne Leadership Class Facility, a DOE Office of Science Facility supported under Contract De-AC02-06CH11357, on the STFC-funded "DiRAC" BG/Q system in the Advanced Computing Facility at the University of Edinburgh, on the BG/Q computers of the RIKEN BNL Research Center and the Brookhaven National Laboratory. The DiRAC equipment was funded by BIS National e-infrastructure capital grants ST/K000411/1, STFC capital grant ST/H008845/1, and STFC DiRAC Operations grants ST/K005804/1 and ST/K005790/1. DiRAC is part of the National e-Infrastructure. C.K. is supported by a RIKEN foreign postdoctoral research (FPR) grant.

References

[1] P. A. Boyle *et al.* [RBC and UKQCD Collaborations], Phys. Rev. Lett. **110**, no. 15, 152001 (2013) [arXiv:1212.1474 [hep-lat]].
[2] Z. Bai *et al.* [RBC and UKQCD Collaborations], Phys. Rev. Lett. **115**, no. 21, 212001 (2015) doi:10.1103/PhysRevLett.115.212001 [arXiv:1505.07863 [hep-lat]].
[3] C. Lehner and C. Sturm, Phys. Rev. D **84**, 014001 (2011) [arXiv:1104.4948 [hep-ph]].
[4] G. Martinelli, C. Pittori, C. T. Sachrajda, M. Testa and A. Vladikas, Nucl. Phys. B **445**, 81 (1995) [hep-lat/9411010].
[5] T. Blum *et al.*, Phys. Rev. D **84**, 114503 (2011) [arXiv:1106.2714 [hep-lat]].
[6] L. Lellouch and M. Luscher, Commun. Math. Phys. **219**, 31 (2001) [hep-lat/0003023].
[7] T. Blum *et al.*, Phys. Rev. Lett. **108**, 141601 (2012) [arXiv:1111.1699 [hep-lat]].
[8] T. Blum *et al.*, Phys. Rev. D **86**, 074513 (2012) [arXiv:1206.5142 [hep-lat]].
[9] R. Arthur *et al.* [RBC and UKQCD Collaborations], Phys. Rev. D **87**, 094514 (2013) [arXiv:1208.4412 [hep-lat]].
[10] T. Blum *et al.* [RBC and UKQCD Collaborations], arXiv:1411.7017 [hep-lat].
[11] T. Blum *et al.*, Phys. Rev. D **91**, no. 7, 074502 (2015) [arXiv:1502.00263 [hep-lat]].
[12] Q. Liu, "*Kaon to Two Pions decays from Lattice QCD: $\Delta I = 1/2$ rule and CP violation*", 2012, ISBN: 9781267290649 [Ph.D. thesis, Columbia University, unpublished]
[13] J. Foley, K. Jimmy Juge, A. O'Cais, M. Peardon, S. M. Ryan and J. I. Skullerud, Comput. Phys. Commun. **172**, 145 (2005) [hep-lat/0505023].
[14] C. h. Kim and N. H. Christ, Nucl. Phys. Proc. Suppl. **119**, 365 (2003) doi:10.1016/S0920-5632(03)01553-6 [hep-lat/0210003].
[15] U. J. Wiese, Nucl. Phys. B **375**, 45 (1992).
[16] C. Kim, Nucl. Phys. Proc. Suppl. **129**, 197 (2004) [hep-lat/0311003].
[17] C. Kelly [RBC and UKQCD collaborations], PoS LATTICE **2012**, 130 (2012).
[18] C. Kelly *et al.* [RBC and UKQCD Collaborations], PoS LATTICE **2013**, 401 (2014).
[19] D. Zhang and C. Kelly, PoS LATTICE **2014**, 366 (2015).
[20] N. Christ, C. Kelly, D. Zhang, "*Lattice simulations with G-parity Boundary Conditions*", in preparation (2015)
[21] C. Kelly and D. Zhang, PoS LATTICE **2014**, 365 (2014).
[22] M. Luscher, Commun. Math. Phys. **105**, 153 (1986).
[23] C. Kim, "*Lattice Calculation of $\Delta I = 3/2$ $K \to \pi\pi$ Decay Amplitude with Interacting Two Pions*", 2004, [Ph.D. thesis, Columbia University, unpublished]
[24] A. Schenk, Nucl. Phys. B **363**, 97 (1991).
[25] G. Colangelo, J. Gasser and H. Leutwyler, Nucl. Phys. B **603**, 125 (2001) [hep-ph/0103088].
[26] G. Colangelo, private communication.
[27] K. Rummukainen and S. A. Gottlieb, Nucl. Phys. B **450**, 397 (1995) [hep-lat/9503028].
[28] C. h. Kim, C. T. Sachrajda and S. R. Sharpe, Nucl. Phys. B **727**, 218 (2005) [hep-lat/0507006].
[29] C. W. Bernard, T. Draper, A. Soni, H. D. Politzer and M. B. Wise, Phys. Rev. D **32**, 2343 (1985). doi:10.1103/PhysRevD.32.2343
[30] G. Buchalla, A. J. Buras and M. E. Lautenbacher, Rev. Mod. Phys. **68**, 1125 (1996) [hep-ph/9512380].